Journal of Materials Chemistry A

RSC Publishing

COMMUNICATION

View Article Online
View Journal | View Issue

Aerosol assisted synthesis of hierarchical tin–carbon composites and their application as lithium battery anode materials†

Cite this: *J. Mater. Chem. A*, 2013, **1**, 8710

Received 23rd May 2013
Accepted 25th June 2013

DOI: 10.1039/c3ta11802a

www.rsc.org/MaterialsA

Juchen Guo,‡* Zichao Yang and Lynden A. Archer*

We report a method for synthesizing hierarchically structured tin–carbon (Sn–C) composites *via* aerosol spray pyrolysis. In this method, an aqueous precursor solution containing tin(II) chloride and sucrose is atomized, and the resultant aerosol droplets carried by an inert gas are pyrolyzed in a high-temperature tubular furnace. Owing to the unique combination of high reaction temperature and short reaction time, this method is able to achieve a hetero-structure in which small Sn particles (15 nm) are uniformly embedded in a secondary carbon particle. This procedure allows the size and size distribution of the primary Sn particles to be tuned, as well as control over the size of the secondary carbon particles by addition of polymeric surfactant in the precursor solution. When evaluated as anode materials for lithium-ion batteries, the resultant Sn–C composites demonstrate attractive electrochemical performance in terms of overall capacity, electrochemical stability, and coulombic efficiency.

Introduction

Metallic tin (Sn) is a promising anode material for Li-ion batteries (LIBs). Its alloying reaction mechanism with lithium (Li) is well understood, $Sn + xLi^+ + xe \leftrightarrow Li_xSn$ ($0 \le x \le 4.4$) and nearly identical to that of silicon (Si). Although Sn has lower gravimetric capacity (992 mA h g^{-1}) compared with Si (4200 mA h g^{-1}), it has comparable volumetric capacity (8322 mA h cm^{-3} of Si *vs.* 7254 mA h cm^{-3} of Sn), which is attractive for most LIB applications.[1] Despite its many merits, progress on developing a superior Sn anode has been slow because the material suffers from inferior cycling stability, which as in the case for Si, has been attributed to large volume swings induced by lithiation and delithiation processes during electrochemical cycling.[2–5] Herein we report a facile, one-step, continuous, and controllable method to synthesize Sn–C composites with hierarchical structures *via* an aerosol spray pyrolysis method. We show that Sn–C composite particles prepared by the approach exhibit exceptional electrochemical stability and attractive coulombic efficiency over hundreds of charge–discharge cycles in a lithium battery.

A variety of methodologies have been developed to impart enhanced resilience to Sn structures targeted for LIB anodes. Among them, porous Sn-based structures[6–8] and Sn encapsulated in hollow carbon structures[2,5,9–12] have attracted significant interest. A drawback of these approaches is that because of the large amounts of void space introduced in the improved designs, improvements in the cycling stability anode typically comes at the expense of its volumetric capacity. Older approaches based on alloying tin with another metal (*e.g.* Sb, Co, Fe, Ni) have been studied continuously for close to two decades[13–19] and have also been demonstrated to provide improvements through the buffering effect provided by extrusion of the second metal during lithiation of Sn. However, the large mass of the buffering phase in most Sn alloys compromise their overall storage capacity. Nanocomposite anodes comprised of Sn and carbon have also attracted significant recent attention as a means of simultaneously improving the mechanical properties and electronic conductivity of Sn-based anodes.[20–24] Sn encapsulated in carbon fibers obtained *via* electrospinning[25,26] stand out for their improved cycling stability, but suffer from processing and materials drawbacks including high unfilled pore volume in the Sn@C fibers, which compromises volumetric capacity of the anode. Considering the literature consensus that the Sn anode fails because of the large cyclic volume changes that accompany lithiation/de-lithiation processes, a rational design for the Sn anode is to uniformly incorporate nanometer-sized Sn particles at high loadings into a resilient and conductive host material. Among the most convincing demonstrations of this concept is the work by Derrien, Scrosati, and coworkers,[4] which shows that Sn–C composites comprised of ~30 nm Sn particles uniformly dispersed in carbon exhibit excellent cycling stability at both low and high discharge rates and high coulombic efficiency. In

School of Chemical and Biomolecular Engineering, Cornell University, Ithaca, NY 14853, USA. E-mail: laa25@cornell.edu; jguo@engr.ucr.edu

† Electronic supplementary information (ESI) available. See DOI: 10.1039/c3ta11802a

‡ Current address: Department of Chemical and Environmental Engineering, University of California at Riverside, Riverside, CA 92521, USA.

particular, the authors showed that infiltration of an organic Sn precursor into a Resorcinol-Formaldehyde (RF) gel, followed by heat treatment in an argon environment can yield Sn–C composites with desirable architectures capable of accommodating the large cyclic strains and stresses produced by repeated lithiation and de-lithiation processes in a LIB anode.

The hierarchical Sn–C particles in this study were synthesized with an aerosol spray pyrolysis apparatus shown in Fig. S1 (ESI†). The method is simple in concept and is adaptable for large scale, continuous production of Sn–C composite particles with favorable mass distributions. Briefly, an aqueous precursor solution containing sucrose (carbon precursor) and $SnCl_2$ (Sn precursor) is fed with a syringe pump into a high-pressure gas enabled atomizer, in which the solution is atomized into small droplets. The droplets are carried by a high-pressure inert gas stream through a diffusion dryer at room temperature, in which most of the water contained in the droplets is removed. The resultant particles composed of sucrose and $SnCl_2$ are transported through a high-temperature tubular furnace at 700 °C to carbonize the sucrose and to transform the $SnCl_2$ to metallic tin. The carbonization and Sn formation steps occur simultaneously in the furnace within a very short residence time of approximately 1 s. The resultant Sn–C composite particles were collected downstream using a porous polymer membrane.

Experimental

Aerosol spray pyrolysis

A single barrel syringe pump was purchased from Chemyx, which was connected to a glass nebulizer purchased from Meinhard. The tip (outlet) of the nebulizer was connected to a homemade diffusion dryer composed of two concentric tubes. The inner tube was made using a stainless steel mesh (12.7 mm diameter, 18 mesh, 70.4% open area) purchased from Direct Metals Co., and the outer tube using commercial poly(vinyl chloride) PVC piping (3.8 cm in diameter). Water adsorbents (silica gel purchased from Sigma-Aldrich) was filled in between the tubes, to create a diffusion drying region approximately 20 cm long. The outlet of the diffusion dryer was connected to a stainless steel tube (0.9 m length and 12.7 mm in diameter), which served as the tubular reactor for the pyrolysis reaction. The tube was heated by a tubular furnace with a single heating zone. The produced particles were collected in a modified Millipore membrane cell with a polypropylene porous membrane (pore size 200 nm). The exhaust gas passing through the membrane was directed to a nearby fume hood.

Composite particle synthesis

In the typical preparation of the precursor solution, 0.46 g of sucrose was added into 20 mL of water (0.067 M) along with 0.38 g of $SnCl_2$ (0.1 M). To prevent the hydrolysis, 0.39 g of 37 wt% HCl (0.2 M) was also added in the solution. To prepare the Sn–$C_{Pluronic}$ composite, 0.85 g of Pluronic F127 (6 time of CMC) was added into the same amount of water with the same amount of $SnCl_2$ and HCl. The amount of sucrose was reduced to 0.34 g (0.05 M), by considering that the tri-block copolymer surfactant could be an additional carbon source. The clear precursor solution was pumped into the nebulizer with a rate of 2 mL h^{-1}. Argon was used as the carrying gas into the nebulizer, and the gauge pressure was 30 psi. The heating temperature of the furnace was 700 °C.

Materials characterization and electrochemical properties

The crystal structures of the composites were characterized using Scintag Theta–theta PAD-X X-ray Diffractometer (Cu Kα, λ = 1.5406 Å). The microstructures of the composites were studied using FEI Tecnai G2 T12 Spirit Transmission Electron Microscope (120 kV). Thermogravimetric analysis (TGA) was performed using TA Instruments Q5000 IR Thermogravimetric Analyzer. The electrochemical characterization of the composites as anode materials in rechargeable lithium batteries was performed at room temperature in two-electrode 2032 coin-type cells. The working electrode consisted of 80 wt% of the active materials, 10 wt% of carbon black (Super-P Li from TIMCAL), and 10 wt% of PVdF (polyvinylidene fluoride, Sigma-Aldrich) as binder. Copper foil (0.004 inch in thickness, Alfa Aesar) was used as the current collector. Lithium foil (0.03 inch in thickness, Alfa Aesar) was used as the counter electrode. 1 M $LiPF_6$ in a mixture of ethylene carbonate, dimethyl carbonate, and diethyl carbonate (1 : 1 : 1 volume ratio) was used as the electrolyte. Celgard 2500 polypropylene membranes were used as the separator. Assembly of cell was performed in a glove box with moisture and oxygen concentrations below 0.1 ppm. The coin cells were cycled using Neware CT-3008 battery testers, and the cyclic voltammetry was performed with a Solartron Model 1470 Potentiostat/Galvanostat.

Results and discussion

Fig. 1 shows the transmission electron spectroscopy (TEM) images of the obtained Sn–C particles. It can be clearly seen that the particles have a hierarchical structure: small primary nanometer-sized Sn particles are dispersed in large secondary carbon particles. In contrast to the secondary particles, which have a broad size distribution (see Fig. 1c), the Sn primary particles are of well-defined sizes (around 15 nm), and are distributed quite uniformly in the carbon framework. The formation and structure of these Sn–C nanocomposite particles is hypothesized to arise from the following thee-stage process. Stage 1: creation of micron-sized aerosol droplets in the atomizer, which comprised of homogenous aqueous solution of the carbon and tin precursors (equivalent HCl was added to the precursor solution to prevent the hydrolysis of $SnCl_2$). Step 2: formation of solid sucrose particles that uniformly encapsulate $SnCl_2$ in the solid state. Stage 3: rapid carbonization of the sucrose and decomposition of $SnCl_2$ in the furnace.

The combination of a high reaction temperature and short reaction/residence time in the furnace is believed to preserve the uniform distribution of $SnCl_2$ during the simultaneous carbonization and Sn formation steps. Additionally, by taking advantage of the small size of the precursor particles and the rapid cooling of the products as they exit the furnace, nanosized Sn particles are formed and the hierarchical structure of the

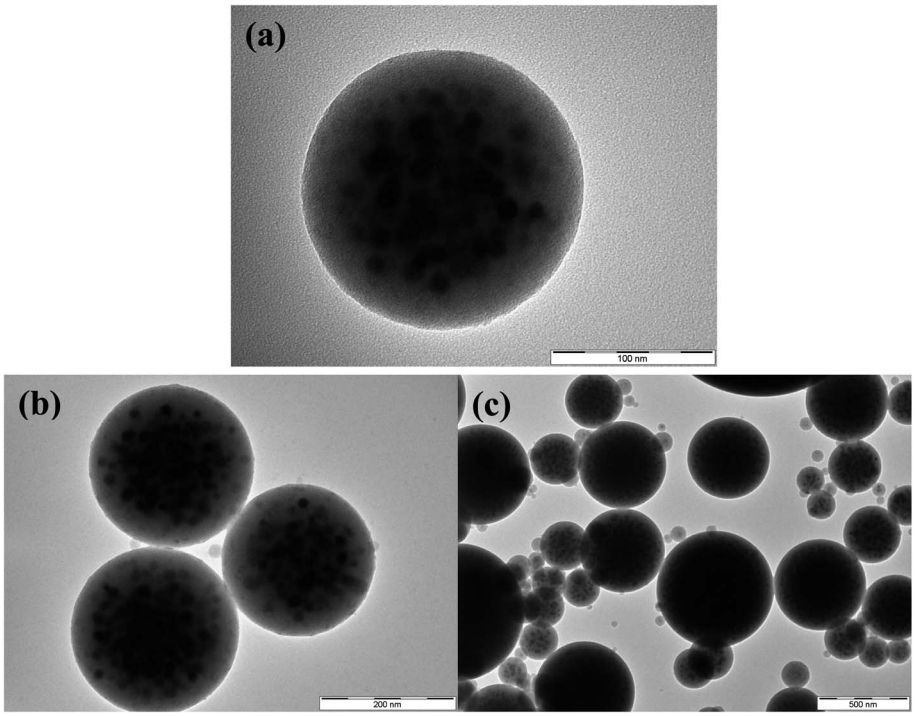

Fig. 1 TEM images of Sn–C particles obtained *via* the aerosol spray pyrolysis method at three magnifications. (a) and (b) illustrate distribution of Sn nanoparticles in ~200 nm carbon spheres; (c) shows that carbon spheres with a broad distribution of sizes are obtained.

composites preserved in the final product. It was found that heating the Sn–C particles at 700 °C for 1 h resulted in hollow carbon particles conjunct to solid Sn particles hundreds of nanometers in size (Fig. S2 in ESI†), confirming the importance of the fast cooling step in preventing melting, leaking, and coalescence (dark black regions in the TEM image in Fig. S2†) of the primary Sn particles. XRD powder patterns of the Sn–C particles are provided in Fig. S3 (ESI†). The results for the Sn–C composite particles are in excellent agreement with expectations for pure elemental Sn phase (JCPDS Card 04-0673). Application of Scherrer's formula to the data provides an estimate for the crystal size of 14 nm, consistent with observations from TEM. In addition to the existence of pure Sn, the XRD pattern of the Sn–$C_{Pluronic}$ composite particles indicate that Sn(II) oxide is present in the composite particles. A possible explanation is that the extra oxygen released upon decomposition of the PEO_{106}-PPO_{70}-PEO_{106} copolymer promoted the oxidation of Sn.

Although the primary Sn nanoparticles obtained using our spray pyrolysis methodology are, as desired, uniformly dispersed in the carbon host, the broad size distribution of the secondary particles is potentially problematic. Such a distribution may result in non-uniformity in the transport path lengths for ions and electrons during electrochemical cycling. To better control the structure of the Sn–C particles, a tri-block copolymer of poly(ethylene glycol)-*block*-poly(propylene glycol)-*block*-poly(ethylene glycol) (Pluronic F127, PEO_{106}-PPO_{70}-PEO_{106}) was studied as a structure directing agent in the precursor solution. The concept was to add the PEO_{106}-PPO_{70}-PEO_{106} surfactant into the precursor solution with a concentration well above its critical micelle concentration (CMC = 0.71 wt% at 25 °C),[27] to create PEO_{106}-PPO_{70}-PEO_{106} micelles in the precursor solution. During the precipitation of the precursors by removing water from the aerosol droplets in the diffusion-drying step, the surface active PEO_{106}-PPO_{70}-PEO_{106} micelles are expected to migrate and precipitate at the shell of the precursor particles. Although the size of the micelles does not directly reflect the particle size of the resultant precursor particles, the PEO_{106}-PPO_{70}-PEO_{106} functions as a regulating agent to produce small particles with well-defined size.

The TEM images of the particles prepared with PEO_{106}-PPO_{70}-PEO_{106} surfactant (denoted as Sn–$C_{Pluronic}$) are shown in Fig. 2. These images provide good support for the above hypothesis. The hierarchical structure of the Sn–$C_{Pluronic}$ is evidently different from the Sn–C particles synthesized without copolymer addition. In particular, structure at three levels is apparent: primary Sn particles with diameters that remain around 15 nm. Secondary carbon particles of approximate size 50 nm, which encapsulate the primary Sn particles. A disordered carbon matrix that encapsulates and is loosely bonded to the secondary carbon particles completes the structure.

The electrochemical properties of Sn–C and Sn–$C_{Pluronic}$ composites were evaluated using cyclic voltammetry (CV) and galvanostatic charge–discharge measurements in coin cells with metallic lithium serving as the counter electrode. A voltage window between 0 V and 1.5 V *vs.* Li/Li^+ and a fixed scan rate of 0.05 mV s^{-1} were employed. As shown in Fig. 3a, the first cathodic scan for the Sn–C composite particles reveals activity over a very broad voltage range, which could be due to the irreversible reaction forming the solid electrolyte interface

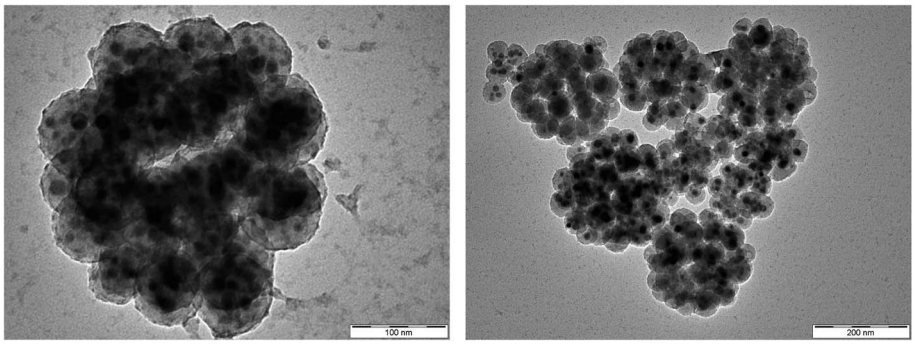

Fig. 2 TEM images of Sn–$C_{Pluronic}$ particles obtained *via* spray pyrolysis method, at two magnifications.

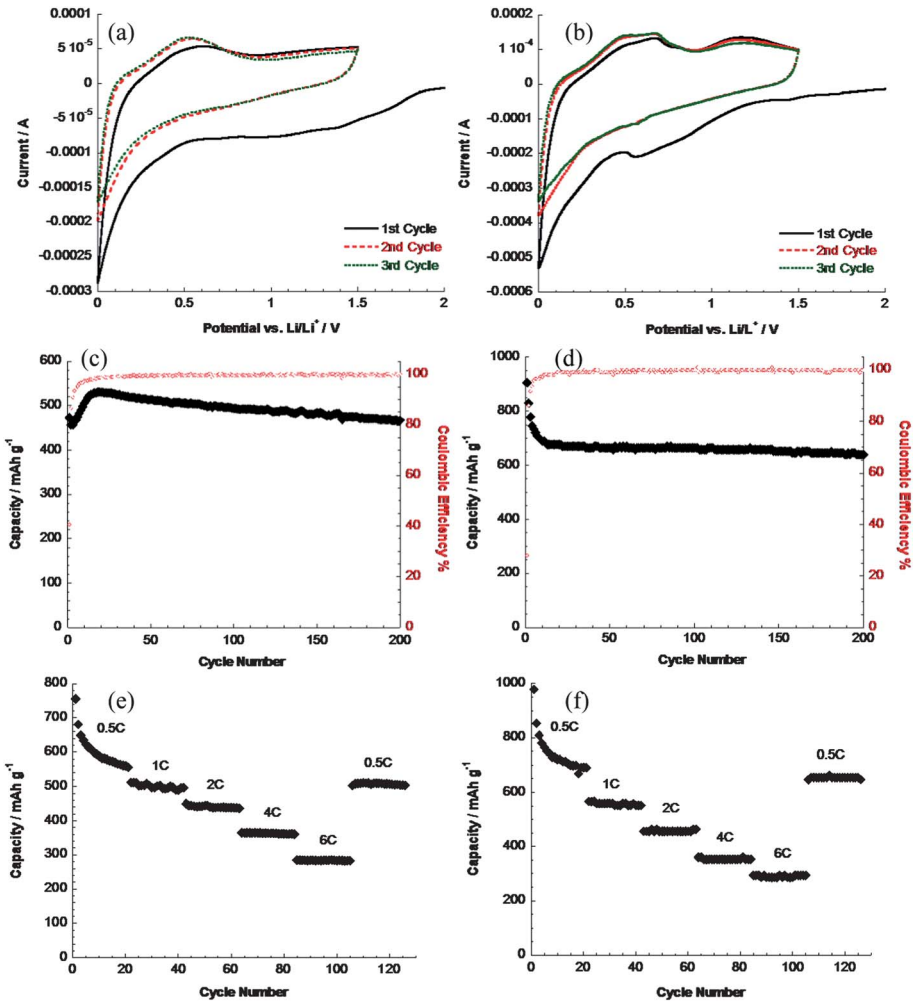

Fig. 3 Cyclic voltammograms between 0 and 1.5 V for: (a) Sn–C and (b) Sn–$C_{Pluronic}$ composite electrodes. A scan rate of 0.05 mV s^{-1} was used for all measurements; galvanostatic discharge capacities and coulombic efficiency for Sn–C and Sn–$C_{Pluronic}$ composites ((c) and (d)), respectively, as a function of cycle number. Measurements were performed at a current density of 500 mA g^{-1} (~1 C) for the materials; rate capability of Sn–C and Sn–$C_{Pluronic}$ composite anodes ((e) and (f)), respectively, measured at current densities ranging from 250 mA g^{-1} to 3000 mA g^{-1}.

(SEI). The broad anodic peak centered at 0.6 V *vs.* Li/Li^+ is believed to be a combination of multiple peaks between 0.5 V and 0.8 V,[28,29] representing different delithiation steps in the various Li–Sn alloys.[14] The second and third CV scans are consistent and indicative of a stabilized lithiation–delithiation process from the second cycle. The first cathodic scan of the Sn–$C_{Pluronic}$ particles (Fig. 3b) shows a cathodic peak at 0.6 V *vs.* Li/Li^+ in addition to the formation the SEI, which can be attributed to the reduction of the residual SnO in the composite.[30] Accordingly, an additional oxidation peak centered

at 1.2 V *vs.* Li/Li^+ was observed in the anodic scans of the $Sn–C_{Pluronic}$ particles, which is consistent with the previously reported oxidation potential of Sn. However, since the reversibility of the Sn–SnO is expected to be sluggish, the peak at 0.6 V may gradually decreases, as indicated by the second and third CV cycles. Also, the irreversibility of this Sn–SnO conversion could explain the capacity drop in the first 10 charge–discharge cycles of $Sn–C_{Pluronic}$ composite, as shown in Fig. 3d.

Fig. 3c and d report the galvanostatic discharge capacity of anodes based on Sn–C and the $Sn–C_{Pluronic}$, respectively. A fixed current density of 500 mA g^{-1} (~1 C) was used for both the charge and discharge processes, and the capacity was calculated based on the total weight of the composites (*i.e.* the total mass of carbon and Sn in the composite materials). It is evident from the figures that both composites exhibit excellent cycling stability, with the Sn–C composite retaining a specific capacity of 470 mA h g^{-1} after 200 cycles. This corresponds to 88% retention, after 200 cycles, of the highest capacity achieved in the cell. The initial coulombic efficiency of the Sn–C composite is 40%, and it quickly improves: the average coulombic efficiency after the 20th cycle is 99.6%. The $Sn–C_{Pluronic}$ material demonstrated even better cycling stability – retaining a capacity of 640 mA h g^{-1} (98% capacity retention from the capacity at the 11th cycle, counting out the effect of SnO) after 200 cycles. The initial coulombic efficiency of $Sn–C_{Pluronic}$ is 30% due to the SnO residue. The average coulombic efficiency after the 20th cycle is 99.9%.

The Sn contents in the Sn–C and $Sn–C_{Pluronic}$ composites were determined by TGA to be 52 wt% and 64 wt%, respectively (Fig. S4 in ESI†). Considering the Sn content of the two composites, it is clear that the materials maintain capacities close to the theoretical values for Sn even after hundreds of charge–discharge cycles, and exhibit minimal irreversible losses and excellent coulombic efficiencies. To our knowledge, these Sn–C and $Sn–C_{Pluronic}$ composites manifest among the best performance of any Sn-based material reported to date. Fig. 3e and f show that the materials also exhibit excellent rate capabilities over a range of consecutive charge–discharges at current densities ranging from 250 mA g^{-1} (0.5 C), 500 mA g^{-1} (1 C), 1 A g^{-1} (2 C), 2 A g^{-1} (4 C), 3 A g^{-1} (6 C), and back to 250 mA g^{-1}. Both electrodes demonstrated similar outstanding rate capacities. For the $Sn–C_{Pluronic}$ composite, its capacity retention at 6 C is 300 mA h g^{-1}, and 96% capacity was recovered when the C rate returned to 0.5 C.

Conclusions

We have synthesized tin–carbon composite anode materials with rationally designed structures aimed at accommodating the large volume changes during lithiation/de-lithiation and at enhancing capacity retention over hundreds of charge–discharge cycles. In particular, we show that a robust aerosol spray pyrolysis method can be used to create hierarchical carbon particles that encapsulate ~15 nm Sn nanostructures uniformly distributed in the carbon host material. The synthesis process is easy to operate and control, and is feasible for large-scale production of the composite anode materials. By adding a tri-block copolymer surfactant as structure directing agent into the precursors, the particle structure of Sn–C composites could be tuned to improve the electrochemical performance. When evaluated as anodes for lithium batteries, the Sn–C composites demonstrate very promising performance; among the best reported to date. We anticipate future efforts aimed at optimizing the composition of the precursors and the operating conditions for the spray pyrolysis process will lead to Sn–C composites with even better morphology control, higher Sn loadings, and improved anode performance.

Acknowledgements

This material is based on work supported as part of the Energy Materials Center at Cornell, an Energy Frontier Research Center funded by the U.S. Department of Energy, Office of Science, Office of Basic Energy Sciences under Award Number DE-SC0001086. This work also received partial support from Award no. KUS-C1-018-02, made by King Abdullah University of Science and Technology (KAUST). Facilities available through the Cornell Center for Materials Research were used for this study.

Notes and references

1 V. L. Chevrier and G. Ceder, *J. Electrochem. Soc.*, 2011, **158**, A1011.
2 X. W. Lou, Y. Wang, C. Yuan, J. Y. Lee and L. A. Archer, *Adv. Mater.*, 2006, **18**, 2325.
3 J. Hassoun, S. Panero, P. Simon, P. L. Taberna and B. Scrosati, *Adv. Mater.*, 2007, **19**, 1632.
4 G. Derrien, J. Hassoun, S. Panero and B. Scrosati, *Adv. Mater.*, 2007, **19**, 2336.
5 X. W. Lou and L. A. Archer, *Adv. Mater.*, 2008, **20**, 1853.
6 Y. Yu, C. Chen and Y. Shi, *Adv. Mater.*, 2007, **19**, 993.
7 S. Chou, J. Wang, H. Liu and S. Dou, *Electrochem. Commun.*, 2009, **11**, 242.
8 R. Liu, N. Li, D. Li, G. Xia, Y. Zhu, S. Yu and C. Wang, *Mater. Lett.*, 2012, **73**, 1.
9 W. Zhang, J. Hu, Y. Guo, S. Zheng, L. Zhong, W. Song and L. Wan, *Adv. Mater.*, 2008, **20**, 1160.
10 X. W. Lou, D. Deng, J. Y. Lee and L. A. Archer, *Chem. Mater.*, 2008, **20**, 6562.
11 Y. Wang, M. Wu, Z. Jiao and J. Y. Lee, *Chem. Mater.*, 2009, **21**, 3210.
12 J. Chen and X. Lou, *Small*, 2013, **9**, 1877.
13 M. Wachtler, J. O. Besenhard and M. Winter, *J. Power Sources*, 2001, **94**, 189.
14 M. Winter and J. O. Besenhard, *Electrochim. Acta*, 1999, **45**, 31.
15 N. Tamura, R. Ohshita, M. Fujimoto, S. Fujitani, M. Kamino and I. Yonezu, *J. Power Sources*, 2002, **107**, 48.
16 X. L. Wang, W. Q. Han, J. J. Chen and J. Graetz, *ACS Appl. Mater. Interfaces*, 2010, **2**, 1548.
17 O. Mao, R. A. Dunlap and J. R. Dahn, *J. Electrochem. Soc.*, 1999, **146**, 405.
18 O. Mao and J. R. Dahn, *J. Electrochem. Soc.*, 1999, **146**, 414.
19 Z. Yang, J. Shen, N. Jayaprakash and L. A. Archer, *Energy Environ. Sci.*, 2012, **5**, 7025.

20 Y. Xu, J. Guo and C. Wang, *J. Mater. Chem.*, 2012, **22**, 9562.
21 Y. Zhao, J. Li, N. Wang, C. Wu, G. Dong and L. Guan, *J. Phys. Chem. C*, 2012, **116**, 18612.
22 X. Li, A. Dhanabalan, L. Gu and C. Wang, *Adv. Energy Mater.*, 2012, **2**, 238.
23 K. Hsu, C. Liu, P. Chen, C. Lee and H. Chiu, *J. Mater. Chem.*, 2012, **22**, 21533.
24 Y. Su, S. Li, D. Wu, F. Zhang, H. Liang, P. Gao, C. Cheng and X. Feng, *ACS Nano*, 2012, **6**, 8349.
25 Y. Yu, L. Gu, C. Wang, A. Dhanabalan, P. A. van Aken and J. Maier, *Angew. Chem., Int. Ed.*, 2009, **48**, 6485.
26 Y. Yu, L. Gu, C. Zhu, P. van Aken and J. Maier, *J. Am. Chem. Soc.*, 2009, **131**, 15984.
27 P. Linse and M. Malmsten, *Macromolecules*, 1992, **25**, 5434.
28 Y. S. Jung, K. T. Lee, J. H. Ryu, D. Im and S. M. Oh, *J. Electrochem. Soc.*, 2005, **152**, A1452.
29 D. Deng and J. Y. Lee, *Angew. Chem., Int. Ed.*, 2009, **48**, 1660.
30 N. Li and C. R. Martin, *J. Electrochem. Soc.*, 2001, **148**, A164.